Indian Journal of Chemistry
Vol. 58A, June 2019, pp. 645-652

Understanding the geometry and [3+2] cycloadditions of nitrile imine in terms of molecular electron density theory

Nivedita Acharjee

Department of Chemistry, Durgapur Government College, J. N. Avenue, Durgapur, West Bengal 713 214, India

Email: nivchem@gmail.com

Received 24 October 2018; revised and accepted 29 April 2019

Nitrile imine has been classified as carbenoid type three atom component (TAC) by coupled cluster single doubles plus perturbative triples (CCSD(T)) calculations. [3+2] cycloaddition (32CA) reactions of nitrile imine with a set of olefins has been studied in this report in terms of Global electron density transfer (GEDT), Bonding evolution theory (BET) and Quantum theory of atoms in molecules (QTAIM) analyses at B3LYP and MPW1K levels. The reactions have been non-polar showing non-covalent interactions and hence GEDT doesn't make the reaction feasible by inducing significant electrophilic-nucleophilic interaction between reactants as occurs in case of polar processes. Mutual penetration of forming bonds to the Van-der Waals' surface has been reproduced in asymmetry indices at the transition states. BET and QTAIM study confirmed initial rupture of olefinic bond, followed by the formation of pseudoradical centres and subsequently the bond-formation processes.

Keywords: Molecular electron density theory, Bonding evolution theory, Nitrile imine, Three atom component

Nitrile imines serve as versatile intermediates in the synthetic processes of five membered heterocycles, especially the 2-pyrazoline derivatives[1]. Biological activity of 2-pyrazoline compounds are well demonstrated in literature[2]. Recently, P An *et al.*,[3] have reported the use of nitrile imine for rapid biorthogonal protein labelling in live cells, where the [3+2] cycloaddition (32CA) reaction of nitrile imine is favored over the competing nucleophilic addition. Nitrile imines are generated in situ for the lifetime of milliseconds, by thermolysis of tetrazoles[4], catalytic oxidation of aldehyde hydrazones[5], dehydrohalogenation of hydrazonoyl chlorides[6] and photolysis of sydnones[7]. Nitrile imines can be captured by ethylene derivatives to provide substituted 2-pyrazolines[8]. Regioselectivity of such reactions has been addressed in different experimental reports[9,10] and recently in terms of DFT based reactivity indices[11].

Theoretical studies by Wong *et al.*,[12] implied that high level ab initio calculations predicted non-planar allenic geometry for the parent nitrile imine HCNHH in ground state (GS). The propargylic geometry with CN triple bond and linear HCN moiety was identified as a transition state for the inversion of the allenic geometry in these calculations. Subsequently, in 2014, Begue *et al.*,[13] reported theoretical studies to explain the geometry of other carbenic nitrile imines using similar calculation systems. The authors reported that propargylic geometry for the ground state is predicted by B3LYP calculations and the non-planar allenic geometry is predicted by CCSD(T) studies.

In 1990, Becke and Edgecombe[14] introduced the concept of Electron Localization Function (ELF) for atomic and molecular systems and stated that ELF depends on total electron density, its gradient and kinetic energy density. Subsequently, a 1994 study published in *Nature*[15] outlined the meaning and use of ELF attractors for classification of chemical bonds. The "*localization attractors*" are defined by the maxima of local quantum mechanical functions related to Pauli exclusion principle. These attractors can be of three basic types: core, bonding and non-bonding. Core attractors surround the atomic nuclei. On the other hand, the bonding attractors are situated between the core attractors. Bond multiplicity is related to the number of bonding attractors. The basin of an attractor is a region of space which contains the points by which a steepest ascent leads to the attractor. Thus, basin of the attractor provides a non-overlapping partition of the space. The three ELF attractors find applications to identify the core, binding and lone-pair regions in a molecular system. Chemical reactions are associated with the breaking and formation of new bonds due to

changes in the specific arrangement of atoms in a molecule. Andrés *et al.*,[16] in 2011 reported the application of ELF to analyze the course of chemical rearrangement. The conventional chemical concepts and quantum mechanical studies were further related by the same research group in a 2016 study[17] by considering electron density transfer studies during a chemical reaction in terms of Bonding Evolution Theory (BET) which requires calculation of total integrating electron density of the ELF basins along the reaction pathway. In the same year, Domingo[18] proposed molecular electron density theory (MEDT) and highlighted the significance of electron density changes along reactions of three atom components (TACs) participating in 32CA reactions. Classification of TACs into pseudodiradical type (pdr-type), pseudo(mono) radical type (pmr-type), carbenoid type (cb-type) and zwitterionic type (zw-type) was provided in this report. Integration of the total electron density at the ELF basins leads to the identification of the presence of pseudoradical centres, bonding regions and non-bonding centres of a TAC and also along reaction coordinates of 32CAs[19]. The global electron density transfer (GEDT)[20] is computed along the reaction to predict the polar or non-polar character and also correlated with the activation energies. MPW[19] system of calculations has been well documented to provide precise predictions for 32CAs in terms of MEDT studies of different TACs. Nitrile imine 32CA reactions serve as easy synthetic pathway for 2-pyrazolines and hence are worth investigating in terms of bonding evolution theory (BET) and quantum theory of atoms in molecules[21] (QTAIM) analyses.

The present study was carried out to present a complete rationalization for structural and electronic aspects of nitrile-imine 32CA reactions to olefins. The investigated reaction scheme is presented in Fig. 1. The nomenclature of atoms has been adapted in accordance to the 2-pyrazoline system throughout the manuscript as shown in Fig. 1. Carbon atom of the nitrile imine is named as C3, nitrogen atom adjacent to C3 is N2 and the other nitrogen atom of nitrile imine is named as N1, thus forming the N1-N2-C3 nitrile imine moiety. For the olefins **2** and **4-9**, C4 and C5 indicate the β and α carbon atoms respectively. For olefin **3** (ethylene), C4 indicates the carbon atom attached to C3 of nitrile imine, while C5 indicates the carbon atom attached to N1 of nitrile imine. The reactions of parent nitrile imine **1** to olefins **2-9** (allowing progressive change from electron releasing to electron withdrawing olefinic substituents with R = Me (**2**), H (**3**), Ph (**4**), $CONH_2$ (**5**), COOMe (**6**), COMe (**7**), CN (**8**) and NO_2 (**9**)) has been studied in terms of BET and QTAIM analyses.

The present study has been divided into four sections:(i) ELF topological analysis of the TAC. (ii) Activation energy and GEDT calculations for the 32CA reactions. (iii) BET study for the reaction of nitrile imine to ethylene. (iv) QTAIM analysis.

Materials and Methods

Computational methods

Geometry of the TAC was optimized at CCSD(T)/6-31G(d), CCSD/6-31G(d), B3LYP/6-311G(d,p) and MPW1K/6-311G(d,p) levels of theory (using the keyword IOp(3/76=0572004280) for MPWPW91/6-311g(d,p) level of theory). Each stationary point was definitely identified for minima with number of imaginary frequencies = 0 or transition states with number of imaginary frequencies = 1. Intrinsic reaction coordinate (IRC) calculations are performed to verify that the energy curve connecting the reactants and products passes through the correct and the lowest TS which must be a first-order saddle point. The global electron density transfer (GEDT)[20] was calculated for each IRC coordinate as GEDT = ΣqA where qA is the net charge and the sum is taken over all the atoms of the nucleophile. The electronic chemical potential μ[22] and chemical hardness η[23] are calculated from the computed ionization potential (I)[24] and electron affinity[24](A). The global electrophilicity index ω is

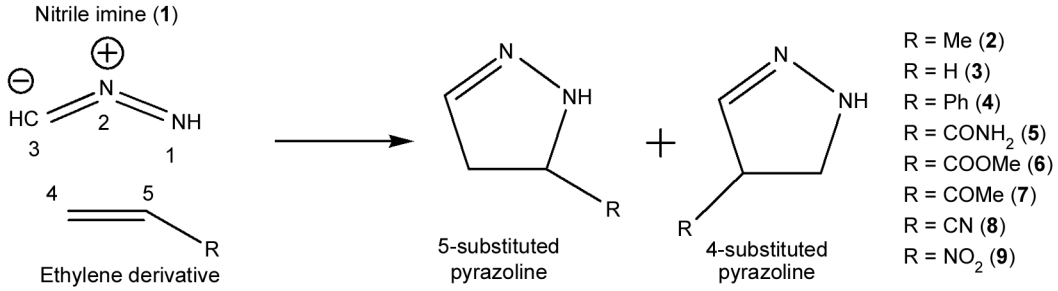

Fig. 1 — 32CA reactions of nitrile imine **1** to olefins **2-9**.

calculated from μ and η using the standard formulae[24,25].

$$\omega = \frac{\mu^2}{2\eta}$$

ELF topological study, QTAIM[21] analysis at the transition states and quantitative analysis of molecular surfaces were performed with Multiwfn[26] software. ELF basin analysis and BET study was performed with high quality grid with spacing 0.06 Bohr. Basins were visualized using Gauss view software. All calculations were carried out using Gaussian 2003[27] set of programs along with the graphical interface Gauss View 2003.

Results and Discussion

ELF topological analysis of the TAC

The bond length and bond angles of optimized TAC at different levels of theory is shown in Fig. 2. B3LYP/6-311G(d,p), MPW1K/6-311G(d,p) and CCSD/6-31G(d) levels show propargylic structure for the TAC. On the other hand, CCSD(T)/6-31G(d) level shows non-planar allenic geometry. Calculations obtained at B3LYP and CCSD(T) levels are in line with the reported observations of Wong *et al.*,[12] and Begue *et al*.[13] Now, considering the ELF study, the ELF attractors are shown in Fig. 3 and basin populations are listed in Table 1.

Each level of calculation shows one V(N1) monosynaptic basin integrating to a total electron density of 3.29 e-3.71 e and also the presence of three disynaptic basins, V(C3, N2), V'(C3,N2) and V(N1-N2). For CCSD/6-31G(d) level, two monosynaptic basins, V(C3) and V'(C3) integrating a total electron density of 0.74 e (each at 0.37 e) is noticed unlike B3LYP and MPW1K levels.

However, for CCSD(T)/6-31G(d) level, one monosynaptic V(C3) basin is shown with total integrating electron population of 1.74 e. Domingo *et al.*,[28] reported ELF study for parent azomethine imine which shows the presence of two monosynaptic basins, V(C3) and V'(C3), integrating a total electron density of 0.62 e, thus characterizing a classification which is neither pseudodiradical nor carbenoid for the TAC and was named as pseudo(mono)radical type (pmr- type). In case of nitrile imine, C3 centre integrating at total density less than 1 e at CCSD/6-31G(d) level, which presents pmr- type classification for nitrile imine by ELF study. On the other hand, B3LYP and MPW1K calculations do not show the presence of any such centre for the TAC. At CCSD(T)/6-31G(d) level, we obtain C3 centre integrating at total density of 1.74 e, thus allowing its classification as carbenoid type (cb- type)[29].

Activation energy and GEDT calculations for 32CAs.

The activation energies calculated at B3LYP/6-311G(d,p) and MPW1K/6-311G(d,p) levels for 32CA reactions of **1** to ethylene derivatives **2-9** are listed in

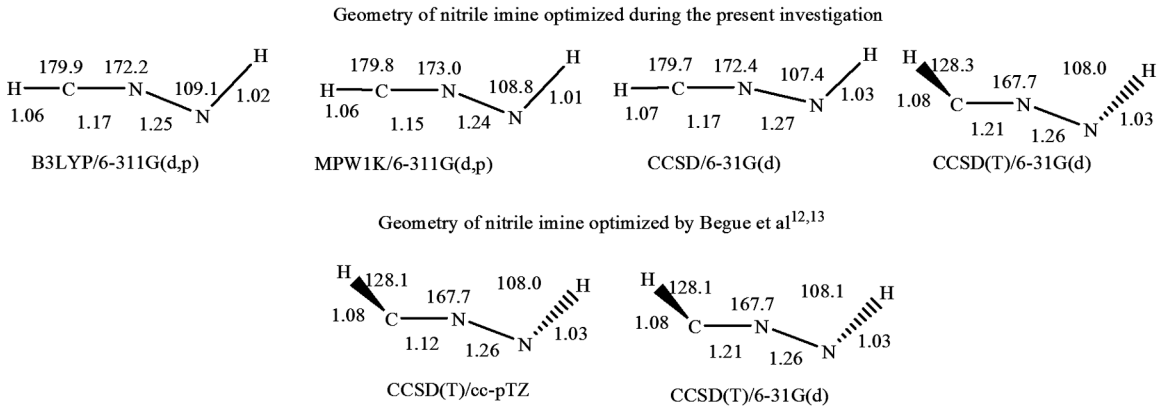

Fig. 2 — Geometry of TAC (nitrile imine) optimized at different theoretical levels.

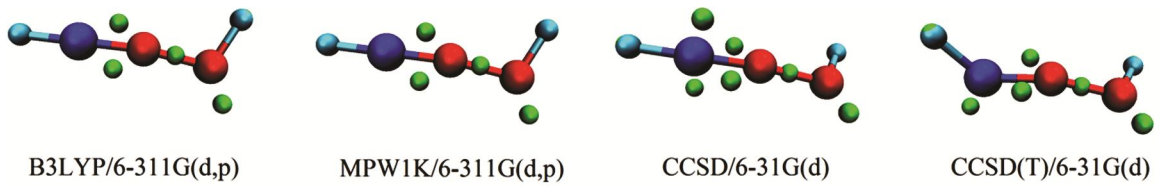

Fig. 3 — ELF attractors of TAC (nitrile imine) at different theoretical levels (Carbon atom is shown in blue, nitrogen in red and hydrogen in light blue colours; attractors are shown as green spheres).

Table 1 — ELF basin population of TAC at different levels

ELF Basins	V(N1)	V(N1-N2)	V(C3-N2)	V'(C3-N2)	V(C3)	V'(C3)	V(C3-H)	V(N1-H)
B3LYP/6-311G(d,p)	3.54	2.21	2.66	2.14	------	------	3.26	1.88
MPW1K/6-311G(d,p)	3.52	2.28	2.64	2.22	------	------	3.14	1.89
CCSD/6-31G(d)	3.71	2.18	2.74	2.22	0.37	0.37	2.23	1.87
CCSD(T)/6-31G(d)	3.29	2.29	2.14	2.22	1.74	------	2.02	1.99

Table 2. **TS1a** to **TS8a** indicate transition states corresponding to the generation of 5-substituted 2-pyrazolines and **TS1b** to **TS8b** indicate transition states leading to 4-substituted 2-pyrazolines. The preference of 5-substituted 2-pyrazolines is evident from the computed data which is in agreement with the general experimental findings[9,10] for nitrile imines. In some cases, the activation energies are comparable to each other.

Global properties of the TAC and ethylene derivatives are listed in Table 3 along with the calculated GEDT for the generation of 5-substituted 2-pyrazolines. In general, the global electrophilicity, ω, increases from **2** to **9** and the electronic chemical potential, μ, generally decreases along the series due to introduction of electron withdrawing olefinic substituent. The calculated magnitudes of (μ_{TAC}–μ_{olefin}) and (ω_{olefin}–ω_{TAC}) generally increases from olefins **2** to **9**. When we carefully consider the global properties of olefins **2** to **9**, we observe deviations in few cases from the general trend. Let us concentrate on μ and ω, which are designated as the DFT based reactivity descriptors for chemical systems[24,25]. The electronic chemical potential μ is calculated from ionization potential and electron affinity according to reference 24 and measures the extent of an electrophile to acquire additional electronic charge. On the other hand, ω depends on μ^2 and η from the standard formula[24,25] and hence considers simultaneously two factors. First, the propensity of the electrophile to acquire additional electronic charge (measured by μ^2) and second, the resistance to exchange electronic charge with the environment (measured by η). A good electrophile is thus expected to have low η value. In the investigated series, from **3** to **4**, both calculation levels show increase in μ value (–3.90 eV to –3.76 eV at B3LYP level) and ω value (0.57 eV to 0.79 eV at B3LYP level). This can probably be attributed to the combined mesomeric and inductive effect of the phenyl substituent which leads to decrease in resistance to share electronic charge (low value of η) in case of **4** compared to **3**, thus resulting in greater electrophilicity of **4** compared to **3,** in spite of its calculated higher μ value. Along the series, both levels show increase in μ value from **6** (= –4.62 eV) to **7** (–4.49 eV) by 0.13 eV at B3LYP level and from **6** (–4.71 eV) to 7 (–4.5 eV) by 0.21 eV at MPW1K level, while ω values of **6** and **7** are comparable to each other and differ by only 0.02–0.03 eV. This observation again dictates the electronic effects of COOMe and COMe substituents, where difference in μ between **6** and **7** is compensated by difference in η values resulting in comparable magnitude of ω for **6** and **7**.

Table 2 — Activation energies for 32CAs of 1 to ethylene derivatives 2-9

32CA	B3LYP/6-311G(d,p)		MPW1K/6-311G(d,p)
	TS	Activation energy (kcal/mol)	Activation energy (kcal/mol)
1 + 2	TS1a	7.09	7.61
	TS1b	8.21	8.57
1 + 3	TS2	5.19	5.67
1 + 4	TS3a	5.06	5.17
	TS3b	7.84	7.41
1 + 5	TS4a	3.9	3.52
	TS4b	4.22	3.66
1 + 6	TS5a	2.95	3.02
	TS5b	2.64	2.83
1 + 7	TS6a	0.78	0.69
	TS6b	3.73	3.10
1 + 8	TS7a	1.94	1.72
	TS7b	4.08	3.26
1 + 9	TS8a	0.68	0.37
	TS8b	1.41	0.55

For 32CA reactions, in general, the activation energy decreases from propene (**2**) to nitroethylene (**9**). However, it is observed that the activation energy from [**1** + **7**]CA to [**1** + **8**] CA deviates from the trend. This can be probably attributed to the extra energy requirement for 32CA reaction of **1** with olefinic bond conjugated to a triple bonded CN substituent unlike other olefins, which probably outweighs the electrophilicity differences.

GEDT values indicate a non-polar process for the reactions of **2** to **9** (GEDT > 0.28 for polar processes). As the reactions are non-polar, theoretical

Table 3 — Global properties of reactants 1-9 and GEDT at the transition states

Reactant	B3LYP/6-311G(d,p)			MPW1K/6-311G(d,p)			TS	GEDT [MPW1K/ 6-311G(d,p)]	GEDT [B3LYP/ 6-311G(d,p)]
	μ (eV)	η (eV)	ω (eV)	μ (eV)	η (eV)	ω (eV)			
1	–3.22	11.34	0.46	–3.17	11.07	0.45			
2	–3.46	12.6	0.47	–3.49	12.49	0.49	TS1a	0.03	0.01
3	–3.90	13.34	0.57	–3.84	13.09	0.56	TS2a	0.05	0.03
4	–3.76	8.98	0.79	–3.77	9.664	0.73	TS3a	0.08	0.05
5	–4.26	10.74	0.85	–4.6	11.67	0.9	TS4a	0.13	0.12
6	–4.62	10.82	0.99	–4.71	10.97	1.01	TS5a	0.13	0.11
7	–4.49	10.01	1.01	–4.5	10.35	0.98	TS6a	0.15	0.13
8	–5.04	11.37	1.12	–5.11	12.17	1.07	TS7a	0.15	0.14
9	–5.71	10.94	1.49	–5.97	11.24	1.59	TS8a	0.17	0.16

Table 4 — MPW1K/6-311G(d,p) calculated bond lengths, asymmetry indices and mutual penetration distance at the transition states

Transition state	Bond length C3-C4 (Å)	Bond length C5-N1 (Å)	Mutual penetration distance (C3-C4) (Å)	Mutual penetration distance (C5-N1) (Å)	Difference in Mutual penetration of C3-C4 and C5-N1 bonds (Å)	Asymmetry index Δa*
TS1a	2.27	2.43	1.59	1.31	0.28	0.12
TS2a	2.30	2.38	1.53	1.33	0.20	0.08
TS3a	2.27	2.45	1.59	1.31	0.28	0.14
TS4a	2.28	2.32	1.57	1.46	0.11	0.05
TS5a	2.25	2.46	1.58	1.28	0.30	0.18
TS6a	2.23	2.53	1.58	1.27	0.31	0.23
TS7a	2.23	2.45	1.59	1.29	0.30	0.17
TS8a	2.22	2.46	1.58	1.26	0.32	0.21

*Calculation of asymmetry index:
I_{C-C}[32] = 1– ({$r^{TS}_{C-C} - r^{P}_{C-C}$}/$r^{P}_{C-C}$) ; I_{C-O} = 1– ({$r^{TS}_{C-O} - r^{P}_{C-O}$}/$r^{P}_{C-O}$)
r^{TS} and r^{P} are the bond distances of TSs and cycloadducts;
Asymmetry index[32], Δa = $I_{C-C} - I_{C-O}$

rationalizations in terms of Parr functions[30] and other regioselectivity descriptors based on electrophilic-nucleophilic interactions could not be employed for the present study. It is evident that with the increase in GEDT from 0.03 to 0.17, the activation energy decreases from 7.09 kcal/mol in propene **2** to 0.68 in nitroethylene **9** at B3LYP level and at MPW1K level the increase in GEDT from 0.01 to 0.16, the activation energy decreases from 7.61 kcal/mol in propene **2** to 0.37 in nitroethylene **9**.

Presently, we have reported the mutual penetration distance of the forming bonds to MEP[31] surfaces for transition states of 32CA of C-phenyl-N-methyl nitrone to ethyl vinyl ether. The mutual penetration distance of the forming bonds is given by the difference between the distance of the non-covalently interacting atom pair and the sum of their non-bonded atomic radius. The larger the distance stronger is the interaction. The non-bonded atomic radius is the closest distance between a nucleus and the molecular Van-der Waals (vdW) surface. For the present study, the mutual penetration distances were calculated and listed in Table 4 along with the bond lengths of the forming C-N and C-C bonds. The forming C-N bond is longer than the forming C-C bond in each case. The asymmetry indices were calculated for the transition states in accordance to Jasiński *et al.*,[32] as shown in Table 4.

The difference in mutual penetration distance between the forming bonds and the asymmetry indices of transition states are shown graphically in Figure 4. It is evident that the mutual penetration distance of the forming bonds and the calculated asymmetry indices of the transition states follow similar pattern of changes along the series. There is drop in asymmetry index for **TS4a** in each case and the maximum value is attained for **TS3a**. It is because, the mutual penetration distance is measured between two non-covalently interacting atom pairs, i.e., (C3 with C4) & (C5 with N1), in this case. This non-covalent interaction dictates the faster generation of one forming bond compared to the other, which is

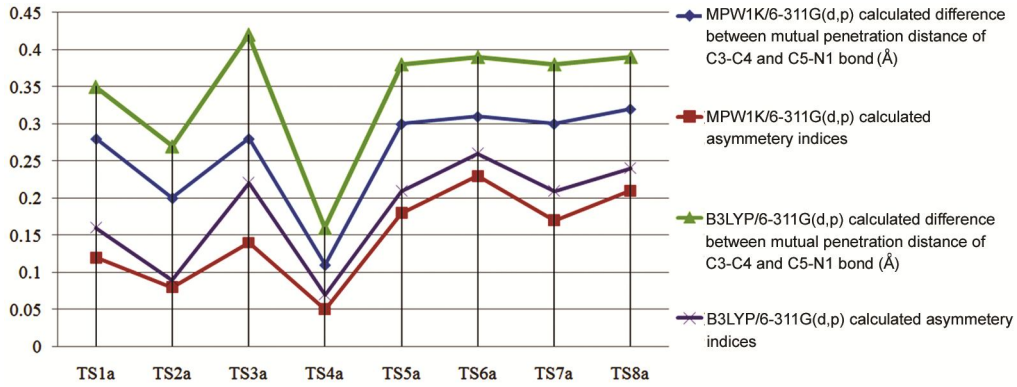

Fig. 4 — Variation of difference in mutual penetration distance of the forming bonds from the molecular electrostatic potential surface and the calculated asymmetry indices along the transition states.

called the asymmetry of bond formation process. This asymmetry is quantitatively measured by the calculated asymmetry indices[32]. Since, it is a non-polar process according to GEDT calculations, the observed asymmetry can be accounted by the non-covalent interactions between the reacting centers. Thus, similar pattern is observed for the mutual penetration distances and the calculated asymmetry indices.

BET study for the reaction of nitrile imine to ethylene

BET study along 32CA of nitrile imine (**1**) to ethylene (**3**) was performed at both B3LYP/6-311G(d,p) and MPW1K/6-311G(d,p) levels of theory. The relative energies for MPW1K/6-311G(d,p) level of theory along IRC coordinates are shown in Fig. 5. Both levels showed similar results. ELF basin populations along the IRC pathways calculated at MPW1K/6-311G(d,p) level of theory is represented in Fig. 6. It is evident that the reaction can be sectioned into eight different phases, A to H. ELF attractors of the representative nuclear configurations for these eight phases are shown in Fig. 7.

Give here is a brief introduction to the changes in ELF basin populations and chemical implications for these eight ELF phases:

Phase A: This phase shows presence of V(C3) and V(N1) monosynaptic basins and V(N1-N2), V(C4-C5), V'(C4-C5), V(C3-N2) and V'(C3-N2) disynaptic basins. The non-planar allenic geometry of nitrile imine is evident in this phase. No bonding region is noticed between **1** and **3**. There is decrease in ELF basin population of V(C3) and V(N1-N2) along the reaction coordinate. [V(C3-N2) + V'(C3-N2)] population remains constant and then increases along this phase.

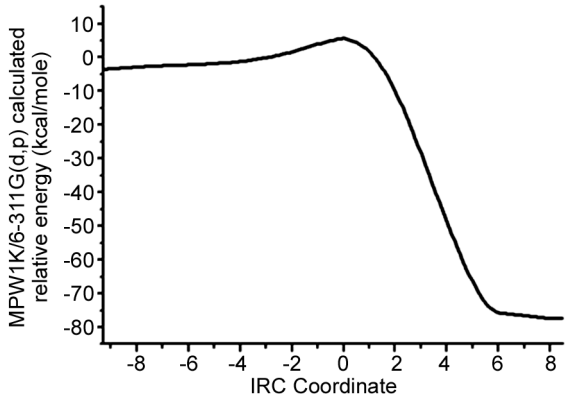

Fig. 5 — MPW1K/6-311G(d,p) calculated relative energies along the IRC coordinate.

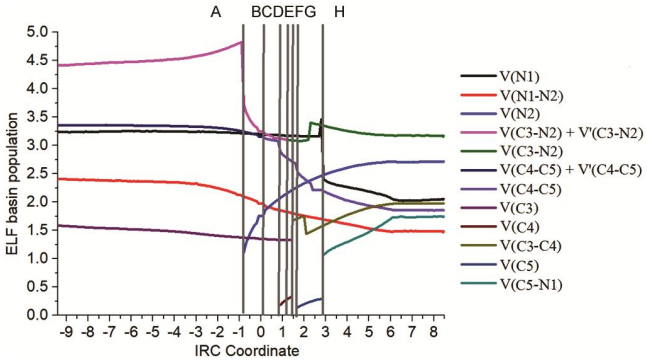

Fig. 6 — MPW1K/6-311G(d,p) calculated ELF basin populations along the IRC Coordinate.

Phase B: In this phase, formation of V(N2) monosynaptic basin integrating at total electron density of 1.116 takes place which increases along the reaction coordinate. There is decrease in [V(C3-N2) + V'(C3-N2)] population. The transition state **TS2a** belongs to this phase. In this stage, although the rupture of C3-N2 bond doesn't take place, but the

formation of V(N2) basin leads to abrupt decrease in its population.

Phase C: In this phase, two V(C4-C5) and V'(C4-C5) basins are no longer visible, instead there is formation of one V(C4-C5) basin. This indicates the rupture of olefinic C4-C5 bond. It is worth mentioning in this context that the reaction being non-polar involves rupture of olefinic bond before the formation of pseudoradical centres along the reaction coordinate.

Phase D: This phase starts with the formation of V(C4) monosynaptic basin and hence implies the generation of a pseudoradical centre at C4. V(C4-C5) population decreases along the phase.

Phase E: In this phase, two V(C3-N2) and V'(C3-N2) basins are no longer visible, instead there is formation of one V(C3-N2) basin. This indicates the rupture of one C3-N2 bond.

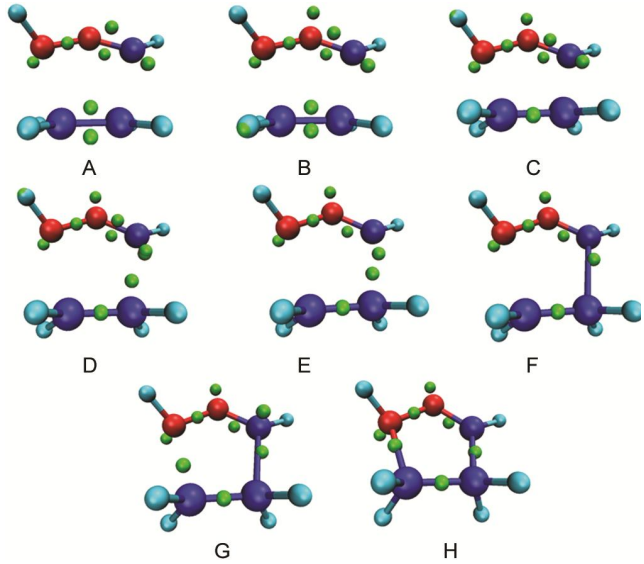

Fig. 7 — MPW1K/6-311G(d,p) calculated ELF attractors of representative examples from phase A to H (Carbon atom is shown in blue, nitrogen in red and hydrogen in light blue colours; attractors are shown as green spheres).

Phase F: In this phase V(C4) basin is no longer visible, instead there is generation of V(C3-C4) basin which indicates the formation of C3-C4 bond.

Phase G: This phase starts with the formation of V(C5) monosynaptic basin and hence implies the generation of a pseudoradical centre at C5.

Phase H: In this phase V(C5) basin is no longer visible, instead there is generation of V(C5-N1) basin which indicates the formation of C5-N1 bond.

QTAIM analysis along the reaction coordinate

QTAIM analysis along a reaction allows the identification of non-covalent/covalent interactions present in a course of reaction. For the present study, QTAIM analysis was performed for (3,–1) bond critical points of the forming C3-C4 and C5-N1 bonds (CP1 and CP2 respectively) at both B3LYP/6-311G(d,p) and MPW1K/6-311G(d,p) levels along the IRC pathway. Both levels provided similar results. QTAIM parameters calculated at MPW1K/6-311G(d,p) level for the representative nuclear configuration of each phase is listed in Table 5. Phase A shows positive laplacian of electron density which indicates no covalent bonding region between nitrile imine and ethylene. Laplacian of electron density for both CP1 and CP2 critical points decreases from phase C to phase H, but show positive value in each case. However, the decrease is quite sharper for CP1 compared to CP2. There is faster earlier generation of C3-C4 bond with negative laplacian of electron density shown in phase F. CP2 shows negative laplacian of electron density in phase H indicating covalent bonding between C5 and N1. It requires to be mentioned here that the transition state shows positive laplacian of electron density and lies far

Table 5 — MPW1K/6-311G(d,p) calculated QTAIM parameters (au) of (3,–1) critical points at selected IRC points

ELF phase	CP1 (C3-C4)			CP2 (C5-N1)		
	Electron Density	Laplacian of electron density	Energy Density	Electron Density	Laplacian of electron density	Energy Density
A	0.0317	0.0622	–0.0020	0.0278	0.070	0.0002
B	0.0403	0.0613	–0.0048	0.0337	0.075	–0.0010
C	0.0577	0.0447	–0.0119	0.0443	0.075	–0.0038
D	0.0726	0.0203	–0.0195	0.0526	0.069	–0.0066
E	0.0813	0.003	–0.0246	0.0574	0.065	–0.0084
F	0.0877	–0.011	–0.0286	0.0608	0.061	–0.0098
G	0.1088	–0.062	–0.0433	0.0721	0.046	–0.0151
H	0.2089	–0.402	–0.148	0.1479	–0.135	–0.0787

before the phases involving C3-C4 and C5-N1 bond formation processes. Thus, QTAIM parameters agree well with the ELF basin analysis of the reaction.

Conclusions

The non-planar allenic geometry of nitrile imine predicted by CCSD(T) calculations in ground state allows its classification as carbenoid type three atom component (TAC). GEDT calculations predict non-polar character of the reaction. The reaction being non-polar occurs by initial rupture of olefinic bond and subsequently the generation of pseudoradical centres at the reacting points, which was confirmed by BET studies. Changes in covalent/non-covalent interactions along the reaction pathway could be monitored and visualized by QTAIM analysis in complete agreement with the BET study. The mutual penetration distance of the forming bonds in MEP maps was reproduced in the asymmetry indices of the transition states.

Supplementary Data

BET data calculated for all 185 nuclear configurations at B3LYP/6-311G(d,p) [Table S1], and 189 nuclear configurations at MPW1K/6-311G(d,p) levels [Table S2] with Standard orientation of reactants [Tables S3 to S14], transitions states [Tables S15 to S22] are provided in supplementary information. Supplementary Data associated with this article are available in the electronic form at http://www.niscair.res.in/jinfo/ijca/IJCA_58A(06)645-652_SupplData.pdf.

Acknowledgement

N Acharjee, is thankful to Professor Luis R Domingo, University of Valencia, Spain and Professor Manas Banerjee (Retired), University of Burdwan, West Bengal, India for kind cooperation and guidance.

References

1 Sharp J T, *The Chemistry of Heterocyclic Compounds Synthetic Applications of 1,3-Dipolar Cycloaddition Chemistry Toward Heterocycles and Natural Products*, (John Wiley & Sons, New York) 2002, p. 473.
2 Kumar K A & Govindaraju M, *Int J Chem Tech Res*, 8 (2015) 313.
3 An P, Lewandowski T M, Erbay T G, Liu P & Lin Q, *J Am Chem Soc*, 140 (2018) 4860.
4 Wentrup C, Dipl C, Fischer S, Maquestiau A & Flammang R, *Angew Chem*, 24 (1985) 56.
5 Gladstone W A F, Aylward J B & Norman R O C, *J Chem Soc C*, (1969) 2587.
6 Huisgen R, Seidel M, Wallbillich G & Knufper H, *Tetrahedron Lett*, 17 (1962) 3.
7 Bhattacharyya K, Ramaiah D, Das P K & George M V, *J Photochem*, 36 (1987) 63.
8 Huisgen R, Grashey R & Sauer J, *Cycloaddition reactions of alkenes in The Chemistry of Alkenes*, (Interscience, New York) 1964, p. 739.
9 Hassaneen H M, Hilal R H, Elwan N M, Harhash A & Shawali A S, *J Heterocyclic Chem*, 21 (1984) 1013.
10 Kumar K A, Govindaraju M & Kumar V G, *Int J Res Pharm Chem*, 3 (2013) 140.
11 Molteni G & Ponti A, *Molecules*, 22 (2017) 202.
12 Wong M W & Wentrup C, *J Am Chem Soc*, 115 (1993) 7743.
13 Begue D & Wentrup C, *J Org Chem*, 79 (2014) 1418.
14 Becke A D & Edgecombe K E, *J Chem Phys*, 92 (1990) 5397.
15 Silvi B & Savin A, *Nature*, 371 (1994) 683.
16 Andrés J, Berski S, Domingo L R, Polo V & B Silvi, *Curr Org Chem*, 15 (2011) 3566.
17 Andrés J, Berski S & B Silvi, *Chem Comm*, 52 (2016) 8183.
18 Domingo L R, *Molecules*, 21 (2016) 1319.
19 Domingo L R, Gutiérrez M R & Pérez P, *J Org Chem*, 83 (2018) 2182.
20 Domingo L R, *RSC Adv*, 4 (2014) 32415.
21 Domingo L R, Gutiérrez M R & Pérez P, *Tetrahedron Lett*, 73 (2017) 1718.
22 Parr R G & W Yang, *Density Functional Theory of Atoms and Molecules*, (Oxford University Press, New York) 1989.
23 Parr R G & Pearson R G, *J Am Chem Soc*, 105 (1983) 7512.
24 Domingo L R, Sáez J A & Pérez P, *Chem Phys Lett*, 438 (2007) 341.
25 Domingo L R, Aurell M J, Perez P & Contreras R, *Tetrahedron Lett*, 58 (2002) 4417.
26 Lu T & Chen F, *J Comp Chem*, 33 (2012) 580.
27 Frisch M J, Trucks G W, Schlegel H B, Scuseria G E, Robb M A, Cheeseman J R, Montgomery Jr JA, Vreven T, Kudin K N, Burant J C, Millam J M, Iyengar S S, Tomasi J, Barone V, Mennucci B, Cossi M, Scalmani G, Rega N, Petersson GA, Nakatsuji H, Hada M, Ehara M, Toyota K, Fukuda R, Hasegawa J, Ishida M, Nakajima T, Honda Y, Kitao O, Nakai H, Klene M, Li X, Knox J E, Hratchian H P, Cross J B, Bakken V, Adamo C, Jaramillo J, Gomperts R, Stratmann R E, Yazyev O, Austin A J, Cammi R, Pomelli C, Ochterski J W, Ayala P Y, Morokuma K, Voth G A, Salvador P, Dannenberg J J, Zakrzewski V G, Dapprich S, Daniels A D, Strain M C, Farkas O, Malick D K, Rabuck A D, Raghavachari K, Foresman J B, Ortiz J V, Cui Q, Baboul A G, Clifford S, Cioslowski J, Stefanov B B, Liu G, Liashenko A, Piskorz P, Komaromi I, Martin R L, Fox D J, Keith T, Al-Laham MA, Peng CY; Nanayakkara A, Challacombe M, Gill P M W, Johnson B, Chen W, Wong M W, Gonzalez C & Pople J A, *Gaussian 03, Rev D.01*, Gaussian, Inc, Wallingford CT, 2004.
28 Domingo L R & Gutiérrez M R, *Molecules*, 22 (2017) 750.
29 Domingo L R, Gutiérrez M R & Pérez P, *Tetrahedron Lett*, 72 (2016) 1524.
30 Domingo L R, Pérez P & Sáez J A, *RSC Adv*, 3 (2013) 1486.
31 Domingo L R & Acharjee N, *Chem Select*, 3 (2018) 8373.
32 Jasiński R, Wąsik K, Mikulskaa M & Barański A, *J Phys Org Chem*, 22 (2009) 717.